Resonance Raman Scattering of Rhodamine 6G as Calculated by Time-Dependent Density Functional Theory: Vibronic and Solvent Effects

Julien Guthmuller* and Benoît Champagne

Laboratoire de Chimie Théorique Appliquée, Facultés Universitaires Notre-Dame de la Paix, Rue de Bruxelles 61, B-5000 Namur, Belgium

Received: November 27, 2007; In Final Form: January 10, 2008

The geometries, UV−vis absorption spectra, and resonance Raman (RR) intensities have been determined for the S_1 and S_3 excited states of rhodamine 6G (R6G) in vacuum and ethanol by means of DFT/TDDFT methodologies with the aim of better understanding the structures and properties of the excited states. The RR spectra have been simulated from the vibronic theory of RR scattering as well as within the short-time approximation, while the solvent effects have been modeled using the polarizable continuum model. The S_1 and S_3 states of R6G present UV−vis absorption bands with similar vibronic structure, i.e., a shoulder at smaller wavelengths, although this shoulder is relatively more intense and more sensitive to the solvent in the case of S_3. These differences are corroborated by the larger geometry relaxations upon excitation for S_3 and the fact that the charge transfer of S_3 is reduced in ethanol. Moreover, the differences between S_1 and S_3 are magnified when considering the RR spectra. On one hand, the RR spectrum of R6G in resonance with the $S_0 \rightarrow S_1$ transition presents many transitions of which the relative intensities strongly vary when the excitation wavelength gets closer to the maximum of absorption. The RR spectrum of R6G in resonance with S_1 is however little influenced by the solvent. On the other hand, the RR spectrum of R6G in resonance with the $S_0 \rightarrow S_3$ transition displays only a few bands, strongly depends on the solvent, and is little affected when changing the excitation wavelength within the limits of the absorption band. As a consequence, the short-time approximation is suitable to reproduce the RR spectrum of R6G in resonance with S_3 for a broad range of excitation wavelengths, whereas the vibronic theory approach is needed for describing the RR spectrum of R6G in resonance with S_1 close to resonance.

1. Introduction

Resonance Raman (RR) spectroscopy[1−8] refers to an inelastic scattering process, where the incident frequency ω_L is in resonance with one of the electronic excited states of the molecule. Since the RR intensities depend on the structural modifications along the normal coordinates of vibration upon excitation to the excited state, this technique has been shown to be efficient to determine the structural properties of the excited states as well as the corresponding energy reorganization occurring upon electronic excitation. For example, RR measurements have been used to investigate the solvent effect of various conjugated chromophores[4,9−13] as well as to study the properties of radical cations.[14,15] The understanding and interpretation of the experimental results can benefit from the use of theoretical models to describe the structural and electronic properties of the ground and excited states. In particular, quantum chemical calculations can provide valuable information on the geometries and vibrations of the ground and excited states, on the vibronic structure of the UV−vis absorption spectra, as well as on the RR intensities and excitation profiles. In general, theoretical models combined with quantum chemistry calculations can be used to interpret a broad range of vibrational spectra,[16] which is also a research direction pursued in our group.[17−23]

In a previous paper[24] we applied density functional theory (DFT) and time-dependent density functional theory (TDDFT) methodologies to analyze the RR properties of the julolidine-malononitrile push−pull chromophore in different solvents. For this compound, it was shown that quantum chemical calculations allow a good description of the absorption and RR spectra and of their solvent dependence. Moreover, the vibronic theory of RR allowed the determination of the RR excitation profiles for various vibrational modes in solution. In this paper, we present an application of the same methodology to the molecule of rhodamine 6G (R6G). R6G is a cationic dye possessing a strong absorption band in the visible domain with its maximum around 530 nm, followed by a weaker band around 350 nm. Its structure consists of a xanthene ring substituted by two methyl groups, two ethylamino groups, and a carboxyphenyl group. In vacuum, the phenyl ring plane is found almost perpendicular to the xanthene plane and therefore not conjugated to it. The properties of R6G have been characterized in several experimental works using different linear and nonlinear spectroscopic techniques. For example, it was used as a probe in surface-enhanced resonance Raman (SERR) measurements[25−30] as well as tip-enhanced near-field Raman (TER) scattering.[31,32] These studies were performed with an excitation wavelength in resonance with the first absorption band. Its linear properties were also investigated by absorption and fluorescence spectroscopies[33−37] in solution. In the case of nonlinear techniques, R6G was studied by surface-enhanced resonance hyper-Raman scattering[27] and doubly resonant sum frequency generation[38,39] in resonance with the first absorption band. Resonant second-harmonic generation measurements[40,41] were also reported and analyzed for an excitation in resonance with the second absorption band. Theoretical studies of R6G using quantum chemical calculations were performed only recently. Watanabe et al.[30] determined the

10.1021/jp7112279 CCC: $40.75
Published on Web 03/08/2008

vibrational frequencies and normal modes of the ground state using DFT in order to interpret Raman, RR, SERR, and TER scattering measurements. In a recent paper Jensen and Schatz[42] simulated the Raman and RR spectra in vacuum employing a TDDFT approach, suitable to evaluate the frequency-dependent polarizability derivatives in both off-resonant and resonant domains.

In this work, we present a TDDFT study of the RR properties of R6G by applying the methodology we previously described for the analysis of the julolidinemalononitrile chromophore.[24] The two states that determine the low-energy UV−vis absorption spectra of R6G are investigated: (1) geometrical changes upon excitation—and therefore geometries of the excited states—are determined within the displaced harmonic oscillator scheme, (2) the vibronic structures of the UV−vis absorption spectra are determined by evaluating the Franck−Condon factors, (3) the RR spectra are simulated using the short-time approximation as well as the vibronic RR theory when assessing the effect of the excitation wavelength, (4) the effects of the solvent (ethanol) on the structures and properties are analyzed using the polarizable continuum model (PCM), and (5) these different simulations are compared to experimental and other theoretical results.

2. Theoretical Method

The resonance Raman intensities were calculated using the vibronic theory expressions of RR scattering derived by Peticolas and Rush.[43] This approach makes use of the following assumptions: (1) the Born−Oppenheimer approximation is valid, (2) only Condon scattering is considered, which corresponds to the A term of Albrecht,[1] (3) the incident light is in resonance with only one excited state at a time, (4) the ground-state and excited-state potential-energy surfaces are harmonic, (5) the excited-state potential-energy surface is only displaced (the frequencies of vibration of the ground and excited states are assumed to be the same, and there are no Duschinsky[44] rotations), (6) the initial state is the vibrational ground state ($\nu = 0$), (7) resonance Raman intensities for overtone and combination bands are not taken into account. Within these assumptions, the RR intensity for the fundamental $0 \rightarrow 1_l$ transition is proportional to the fourth power of the electronic transition moment (M_{0e}) and a frequency-dependent term given by[43,45]

$$I_{0\rightarrow 1_l}(\omega_L) \propto \omega_L(\omega_L - \omega_l)^3 \frac{\Delta_l^2}{2} |\Phi(\omega_L) - \Phi(\omega_L - \omega_l)|^2 \quad (1)$$

where ω_L is the frequency of the incident light, ω_l is the frequency of the lth normal vibrational mode, Δ_l is the dimensionless displacement for the lth normal coordinate, and the function $\Phi(\omega_L)$ is given by the expression

$$\Phi(\omega_L) = \sum_u \frac{\prod_i^{3N-6} |\langle \chi_{g0_i} | \chi_{eui} \rangle|^2}{\omega_{e0,g0} + \sum_j^{3N-6} u_j\omega_j - \omega_L - i\Gamma} \quad (2)$$

where the summation over u is taken over all the vibrational quantum numbers u_i of the probed electronic excited state, $\omega_{e0,g0}$ is the Bohr frequency of the origin transition, $\langle \chi_{g0_i} | \chi_{eu_i} \rangle$ is the one-dimensional overlap integral between the ground state g and the excited state e for the ith normal mode, and Γ is a damping factor describing a homogeneous broadening. This factor is equal to one-half of the full width at half-maximum (fwhm) of the Lorentzian line shape and assumed to be the same for all vibronic levels.

A simplification[43] of eq 1 can be obtained by neglecting the dependence on the excitation frequency ω_L

$$I_{0\rightarrow 1l} \propto \omega_l^2 \Delta_l^2 \quad (3)$$

This expression was earlier derived by Heller and co-workers[46,47,2] from the time-dependent formulation of RR scattering in the short-time dynamics limit and is therefore referred to as the short-time approximation.

The absorption spectrum $A(\omega_L)$ of the excited state can be evaluated from the imaginary part[48,49] of the $\Phi(\omega_L)$ function

$$A(\omega_L) \propto \omega_L Im\Phi(\omega_L) \quad (4)$$

Prediction of the RR intensities and the absorption spectrum requires calculation of the dimensionless displacements Δ_l. Assuming displaced harmonic oscillators, these quantities were determined from the partial derivatives of the excited-state electronic energy along the normal modes at the ground-state equilibrium position. These displacements allow the evaluation of the Franck−Condon overlap integrals from an analytic expression[24] as well as the geometry of the excited state by a transformation between the dimensionless displacements Δ_l and the non-mass-weighted Cartesian coordinates (for more details, see ref 24). The RR intensities were calculated either from the short-time approximation expression (eq 3) or the frequency-dependent expression (eq 1) assuming a fixed value of ω_L. The quantities $|\Phi(\omega_L) - \Phi(\omega_L - \omega_l)|^2$ and $Im\Phi(\omega_L)$ appearing in eqs 1 and 4, respectively, were calculated from their sum-over-vibrational-states expressions given by eq 2. Finally, the damping factor Γ and the Bohr frequency $\omega_{e0,g0}$ were considered as adjustable parameters chosen to reproduce both the experimental absorption spectrum broadening and the position of the absorption maximum.

Quantum chemical calculations were carried out using the GAUSSIAN 03 program.[50] The geometries and frequencies of vibration in the ground state were obtained by means of density functional theory using the B3LYP[51,52] exchange-correlation (XC) functional with the 6-311G* basis set, which contains d polarization functions on the C, N, and O atoms. The vertical excitation energies and oscillator strengths were calculated at the TDDFT level within the adiabatic approximation with the same functional and basis set. The effect of the solvent (ethanol) on the geometries, frequencies, and transition excitations was taken into account by the integral equation formalism of the polarizable continuum model[53−55] (IEFPCM). In this model the solute is placed in a molecular-shaped cavity surrounded by the solvent. The cavity was built using the radii given by the united atom topological model (UA0). The nonequilibrium procedure of solvation was used for the calculation of excitation energies. This model is well adapted for processes in which only the fast reorganization of the electronic distribution of the solvent should be taken into account. The theoretical vibrational normal-mode frequencies were corrected using a scaling factor of 0.98 in order to better match the experimental frequencies given in ref 30.

3. Results

3.1. Excited States. Table 1 presents the vertical energies and oscillator strengths of the six lowest excited states of R6G. The states are found with a different energy order in vacuum and ethanol. However, they can be unambiguously identified

TABLE 1: Vertical Excitation Energies, Oscillator Strengths, and Singly Excited Configurations with Weights Larger than 10% for the Six Lowest Singlet Excited States of Rhodamine 6G Calculated at the TDDFT/B3LYP/6-311G* Level of Approximation[a]

		vacuum			ethanol				
		theory			theory			experiment[b]	
state	transition	weight (%)	E_{vert} (eV)	f	weight (%)	E_{vert} (eV)	f	E_{max} (eV)	λ_{max} (nm)
S_1	H → L	76	2.89	0.744	78	2.76	0.897	2.34	530
S_2	H-1 → L	86	3.25	0.001	86	3.22	0.002		
S_3	H-2 → L	67	3.74	0.127	77	3.81	0.187	3.56	348
	H → L + 1	12							
S_4	H-3 → L	82	3.75	0.003	89	3.83	0.005		
	H-4 → L	17							
S_5	H → L + 1	87	3.78	0.034	99	3.55	0.002		
S_6	H-4 → L	82	3.86	0.003	89	3.96	0.003		
	H-3 → L	17							

[a] The effects of the solvent (ethanol) are described using the IEFPCM approach. H and L correspond to the highest occupied and lowest unoccupied molecular orbital, respectively. [b] The experimental values are taken from ref 56.

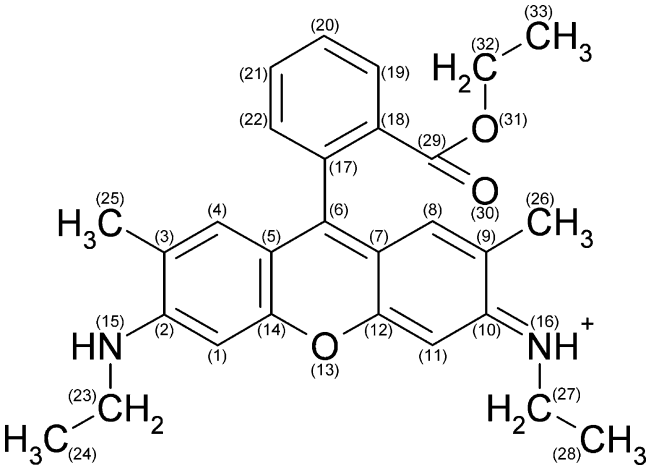

Figure 1. Structure of rhodamine 6G and atomic numbering.

from their dominant singly excited configuration and oscillator strengths. For a matter of facility, they were numbered according to their energy ordering in vacuum. Two states with large oscillator strengths (S_1 and S_3) are found below 4 eV and therefore responsible for the main features of the absorption spectrum in this energy domain. Additional states with small oscillator strengths were also determined with energies close to S_3. Accounting for the solvent effects leads to a bathochromic shift of S_1 by 0.13 eV but a hypsochromic shift of S_3 by 0.07 eV. This opposite behavior of the $S_0 \rightarrow S_1$ and $S_0 \rightarrow S_3$ transitions can be understood when analyzing the main singly excited configurations contributing to S_1 and S_3 (see Table 1 and Figure 2 with the molecular orbitals). Indeed, the non-negligible charge-transfer character of the S_3 state in vacuum, associated with the H → L+1 configuration, is strongly reduced in ethanol. In comparison to vacuum, the oscillator strengths of both S_1 and S_3 states are larger in ethanol with values of 0.897 and 0.187, respectively. Comparisons with the experimental absorption maxima in ethanol[56] show that the calculations overestimate the energy of the S_1 and S_3 states by 0.42 and 0.25 eV, respectively. Indeed, the theory predicts the vertical transitions of the S_1 and S_3 states at 2.76 and 3.81 eV in ethanol, whereas the experimental maxima are found at 2.34 and 3.56 eV for S_1 and S_3, respectively. These discrepancies are typical for TDDFT methods and can be ascribed to the approximate exchange-correlation functional as well as to the lack of vibronic effects.[57] Thus, employing the BP86 pure-DFT XC functional, values of 2.62 and 2.44 eV for the vertical transition of S_1 have been reported in ref 42 in vacuum and water, respectively. Due to their small oscillator strengths, states S_2, S_4, S_5, and S_6 are

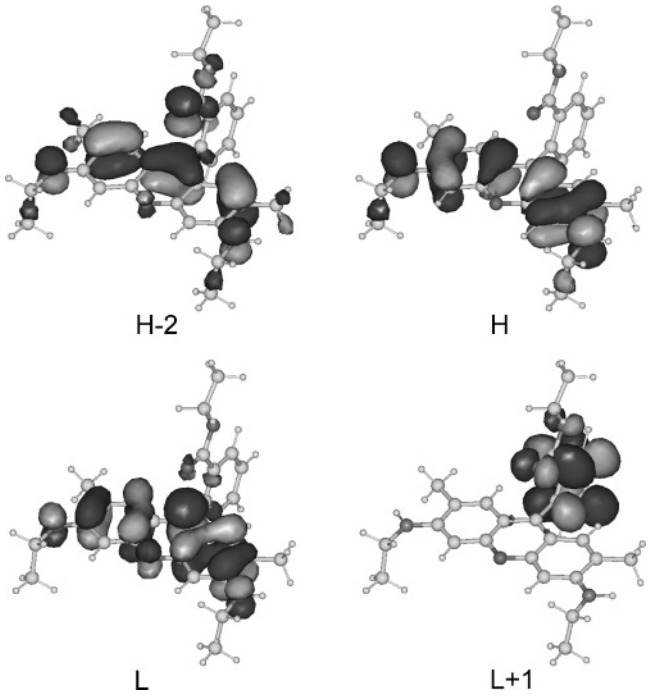

Figure 2. Molecular orbitals involved in the dominant configurations of states S_1 and S_3. H and L correspond to the highest occupied and lowest unoccupied molecular orbital, respectively.

expected to provide negligible contributions to the absorption spectrum and have weak RR intensities. Therefore, in the following, the investigation is restricted to the vibronic structure and resonance Raman properties of the S_1 and S_3 states in vacuum and ethanol.

3.2. Geometries. Table 2 lists the geometrical parameters calculated in vacuum and ethanol for the ground state as well as for the S_1 and S_3 excited states. The atomic numbering used for the bond lengths is given in Figure 1 and similar to the one introduced by Watanabe et al.[30] Though the calculations were performed without symmetry constraint, the geometries of the various states present a plane of symmetry containing the phenyl-COOEt group and perpendicular to the xanthene chromophore. The ground-state geometry is in close agreement with the calculation reported in ref 30 at the B3LYP/6-311++G(d,p) level of approximation. The differences for the bond lengths between the two calculations are smaller than 0.002 Å, except for the C17−C18 bond, which is found to be 0.008 Å longer in our calculation. The effect of the solvent on the

TABLE 2: Ground- (G.S.) and Excited-State (S_1, S_3) Bond Lengths (BL) Calculated at the B3LYP/6-311G* Level of Approximation in Vacuum and Ethanol[a]

	vacuum					ethanol				
	G.S.	S_1		S_3		G.S.	S_1		S_3	
bond	BL (Å)	BL (Å)	ΔBL (Å)	BL (Å)	ΔBL (Å)	BL (Å)	BL (Å)	ΔBL (Å)	BL (Å)	ΔBL (Å)
C1−C2	1.407	1.413	0.006	1.408	0.001	1.410	1.417	0.007	1.410	$<5.10^{-4}$
C1−C14	1.379	1.381	0.002	1.380	0.001	1.378	1.379	0.001	1.382	0.004
C2−C3	1.446	1.438	−0.008	1.435	−0.011	1.448	1.440	−0.008	1.433	−0.015
C2−N15	1.353	1.361	0.008	1.370	0.017	1.351	1.358	0.007	1.376	0.025
C3−C4	1.368	1.379	0.011	1.387	0.019	1.368	1.379	0.011	1.398	0.030
C3−C25	1.506	1.505	−0.001	1.505	−0.001	1.505	1.503	−0.002	1.502	−0.003
C4−C5	1.424	1.422	−0.002	1.415	−0.009	1.424	1.422	−0.002	1.411	−0.013
C5−C6	1.408	1.427	0.019	1.428	0.020	1.407	1.426	0.019	1.433	0.026
C5−C14	1.419	1.420	0.001	1.422	0.003	1.419	1.421	0.002	1.421	0.002
C6−C17	1.496	1.487	−0.009	1.481	−0.015	1.495	1.487	−0.008	1.481	−0.014
O13−C14	1.358	1.366	0.008	1.369	0.011	1.359	1.369	0.010	1.374	0.015
N15−C23	1.463	1.458	−0.005	1.456	−0.007	1.464	1.460	−0.004	1.455	−0.009
C17−C18	1.409	1.412	0.003	1.416	0.007	1.410	1.413	0.003	1.419	0.009
C17−C22	1.398	1.400	0.002	1.398	$<5 \times 10^{-4}$	1.398	1.401	0.003	1.409	0.011
C18−C19	1.400	1.401	0.001	1.405	0.005	1.401	1.402	0.001	1.400	−0.001
C18−C29	1.496	1.498	0.002	1.479	−0.017	1.494	1.496	0.002	1.492	−0.002
C19−C20	1.390	1.390	$<5 \times 10^{-4}$	1.388	−0.002	1.390	1.390	$<5 \times 10^{-4}$	1.397	0.007
C20−C21	1.392	1.392	$<5 \times 10^{-4}$	1.396	0.004	1.393	1.393	$<5 \times 10^{-4}$	1.402	0.009
C21−C22	1.393	1.393	$<5 \times 10^{-4}$	1.396	0.003	1.393	1.393	$<5 \times 10^{-4}$	1.395	0.002
C23−C24	1.531	1.534	0.003	1.536	0.005	1.531	1.535	0.004	1.539	0.008
C29−O30	1.211	1.211	$<5 \times 10^{-4}$	1.229	0.018	1.214	1.214	$<5 \times 10^{-4}$	1.226	0.012
C29−O31	1.338	1.341	0.003	1.329	−0.009	1.340	1.343	0.003	1.343	0.003
O31−C32	1.456	1.454	−0.002	1.467	0.011	1.454	1.453	−0.001	1.466	0.012
C32−C33	1.512	1.513	0.001	1.511	−0.001	1.513	1.513	$<5 \times 10^{-4}$	1.520	0.007

[a] The bond length variations are defined as $\Delta BL_i = BL_i$(excited state) − BL_i(ground state). Due to the plane of symmetry, only the nonredundant values are reported.

ground-state geometry of R6G is rather small. Indeed, the bond lengths are modified by less than 0.004 Å.

The geometries of the S_1 and S_3 excited states as well as the bond length variations, ΔBL = BL(excited state) − BL(ground state), between the ground state and the excited states are reported in Table 2. It appears that the first excited state displays a very similar geometry in vacuum and ethanol. The largest solvent impact on the geometry is found for the C1−C2 bond with a value of 0.004 Å. The geometrical variations ΔBL are also comparable in both environments and differ at most by 0.002 Å. The largest value of ΔBL is obtained for the C5−C6 bond with a variation of 0.019 Å. Additional variations with amplitudes around 0.01 Å are found for the bonds C1−C2, C2−C3, C3−C4, and O13−C14 localized on the xanthene chromophore as well as for the bonds C2−N15 and C6−C17 connecting the ethylamino groups and the phenyl ring to the xanthene, respectively. Therefore, from the geometrical analysis of S_1, it is expected that the RR spectra in vacuum and ethanol will show similar features with enhanced intensities for vibrations involving distortions of the xanthene unit.

The solvent effects on the geometry of S_3 are more pronounced than for S_1. For example, the strongest modifications are found for the bonds C29−O31, C18−C29, C17−C22, and C3−C4, which on going from vacuum to ethanol are lengthened by 0.014, 0.013, 0.011, and 0.011 Å, respectively. This is in agreement with the charge-transfer character of S_3 and its reduction in ethanol. The ΔBL values are in general larger than for S_1 and present noticeable differences in both environments. The largest ΔBL are obtained for the bonds C3−C4, C5−C6, and C2−N15 with values of 0.030, 0.026, and 0.025 Å in ethanol, respectively. Additionally, significant ΔBL values are also found for the bonds C2−C3, C4−C5, C6−C17, O13−C14, C29−O30, and O31−C32. Finally, one can notice a marked difference of ΔBL values between vacuum and ethanol for the bond C17−C22 as well as for the bond C18−C29 linking the phenyl ring to the ethoxy carbonyl group. Contrary to S_1, the pronounced differences obtained in vacuum and ethanol for the ΔBL values of S_3 should lead to distinct absorption and RR spectra in both environments.

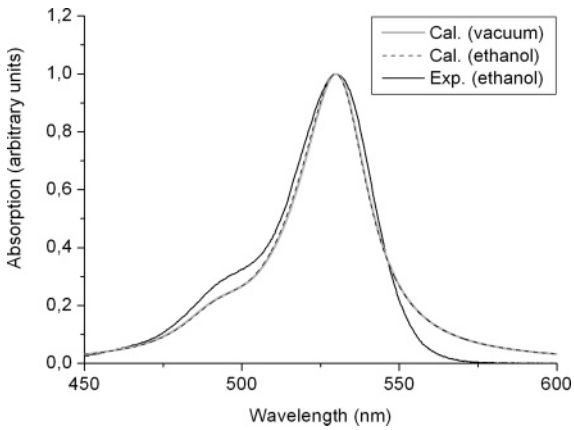

Figure 3. Absorption spectra of the S_1 excited state in vacuum and ethanol. The theoretical spectra (B3LYP/6-311G*) are obtained from eq 4 using a fwhm set to 800 cm^{-1}. The experimental spectrum in ethanol has been taken from ref 56. The theoretical $\omega_{e0,g0}$ origin has been shifted so that experimental and theoretical absorption maxima coincide.

3.3. UV−Vis Absorption Spectra. The absorption spectra of the states S_1 and S_3 evaluated in vacuum and ethanol are reported in Figures 3 and 4, respectively. These spectra are calculated from eq 4 assuming a fwhm of 800 cm^{-1}, which is chosen in order to reproduce the experimental broadening in ethanol. Since no experimental absorption spectrum is available in the gas phase for R6G and even if the broadening in vacuum might be different than that in ethanol, the same value of the fwhm has been taken for both theoretical spectra. To allow an easier comparison, the value of the origin $\omega_{e0,g0}$ is set so that the theoretical and experimental absorption maxima coincide. Furthermore, the amplitudes of the theoretical maxima are

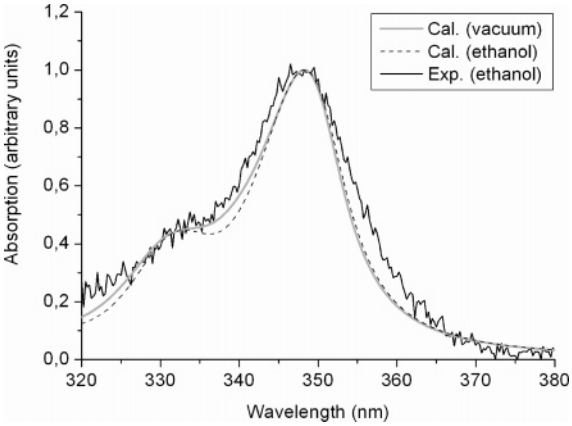

Figure 4. Absorption spectra of the S_3 excited state in vacuum and ethanol. The theoretical spectra (B3LYP/6-311G∗) are obtained from eq 4 using a fwhm set to 800 cm^{-1}. The experimental spectrum in ethanol has been taken from ref 56. The theoretical $\omega_{e0,g0}$ origin has been shifted so that experimental and theoretical absorption maxima coincide.

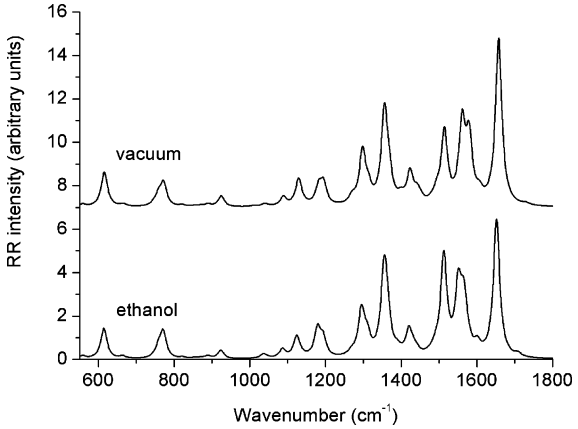

Figure 5. Simulated RR spectra of R6G in resonance with the $S_0 \rightarrow S_1$ transition in vacuum and ethanol (within the short-time approximation) using DFT and TDDFT methods at the B3LYP/6-311G∗ level of approximation. The RR transitions are represented by Lorentzian functions having fwhm of 20 cm^{-1}.

normalized to adjust to the experimental one. A sufficient number of Franck−Condon factors were evaluated to reproduce the main vibronic features of the absorption spectra. The summation of these factors leads to a value close 0.99 for the S_1 state and values of 0.93 and 0.71 for the S_3 state in vacuum and ethanol, respectively. The missing Franck−Condon factors for S_3 are mainly responsible for the background of the absorption spectrum and therefore not essential for the description of the vibronic structure.

For S_1 good agreement is found between the simulated spectra and the measurement carried out in ethanol. Indeed, the experimental vibronic shoulder close to 500 nm is reproduced by the theory in vacuum and ethanol. Its relative intensity with respect to the maximum, with a value around 0.30 in the experiment, is slightly underestimated by the calculations, with a value around 0.25 in both environments. No noticeable differences are obtained between the theoretical spectra in vacuum and ethanol. This similarity is in agreement with the small geometrical differences found for the S_1 state in both environments. Therefore, for this state, it is expected that the solvent will have a weak impact on the RR intensities. The underestimation of the amplitude of the shoulder around 500 nm can have various origins. First, this difference can arise from the approximations made in the theoretical method, particularly the choice of the XC functional. For example, the effect of exact Hartree−Fock exchange in the XC functional has been investigated in a previous paper[24] for a push−pull chromophore. It has been shown that varying the amount of exact Hartree−Fock exchange in the XC functional can modify the vibronic structure. However, in the case of R6G, where the donor and acceptor groups are weakly conjugated, this effect is expected to be smaller and the B3LYP XC functional appears sufficient. A second hypothesis is the presence of a small concentration of molecular dimers in the experimental solution. Indeed, it is known[33−37] that R6G is likely to form dimers—of which the quantity is related to the concentration of monomers in the solution—and that excitonic coupling in these H aggregates is responsible for a relative increase of the shoulder intensity with respect to the main band.[34] Nevertheless, the rather good agreement obtained between the theoretical and experimental results (Figure 3) demonstrates that the shoulder close to 500 nm in the experimental ethanol spectrum mainly originates from the vibronic structure of the monomer. Finally, neglect of inhomogeneous broadening in the theoretical model might also explain some of the deviations between the calculated and the experimental spectra in solution.

Figure 4 presents the absorption spectra of state S_3. Similar to S_1, good agreement is found between theory and experiment. A marked vibronic shoulder is obtained close to 330 nm with a relative intensity with respect to the maximum of absorption of about 0.45 both in the calculated and experimental spectra. This shoulder has a stronger intensity than the shoulder of the S_1 state, which can be associated with the large ΔBL values found for S_3 (Table 2). However, contrary to state S_1, the calculated spectra in vacuum and ethanol are not completely superimposed but show noticeable differences for wavelengths around the vibronic shoulder. In fact, accounting for the solvent leads to a shoulder with a more pronounced shape, which can be understood as a consequence of the larger geometrical differences ΔBL found for this state in ethanol. These differences will also be apparent in the RR spectrum, which provides a more complete picture of the structural modifications occurring upon excitation. Furthermore, the two theoretical spectra are in similar agreement with experiment. Indeed, due to their relatively small deviations and the limited resolution of the experimental absorption spectrum, it is not possible to draw further conclusions concerning the accuracy of the predicted solvent effects.

Finally, the good agreement obtained between the simulated vibronic structures and the experimental absorption spectra validates the geometries calculated for the two excited states S_1 and S_3.

3.4. Resonance Raman Spectra. The RR properties of state S_1 are now addressed. Figure 5 compares the RR spectra obtained in vacuum and ethanol within the short-time approximation. The RR intensities have been obtained from eq 3 without normalization and represented by a Lorentzian function with a fwhm of 20 cm^{-1}. As suggested by the similarities in the geometries and absorption spectra of S_1, the RR spectra display comparable intensities in vacuum and ethanol. Going from vacuum to ethanol, the main differences consist in a decrease of the intensity of the band around 1650 cm^{-1} and a modification of the relative intensities of the bands between 1500 and 1600 cm^{-1}. Therefore, it appears that the ethanol solvent has a rather weak effect on the various properties (geometry, vibronic structure, and RR spectrum) of the S_1 state.

Figure 6 provides a comparison between the calculated RR spectra and the experimental spectrum recorded in ethanol by

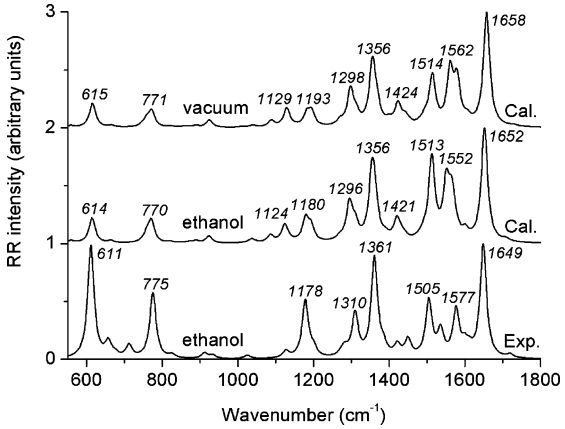

Figure 6. Comparison between theoretical (within the short-time approximation) and experimental RR spectra of R6G in resonance with the $S_0 \rightarrow S_1$ transition. The experimental spectrum in ethanol is constructed from the relative intensities reported in Table 3 of ref 30. The RR transitions are represented by Lorentzian functions having fwhm of 20 cm^{-1} and are normalized so that the intensity of the band around 1650 cm^{-1} is equal to unity.

Watanabe et al.[30] The experimental RR spectrum has been reconstructed from the relative intensities given in Table 3 of ref 30 by applying to each transition a Lorentzian function with a fwhm of 20 cm^{-1}. To allow an easier comparison, the spectra were normalized such that the intensity of the band close to 1650 cm^{-1} is equal to unity. The agreement between the theoretical and experimental spectra is noticeable. With the exception of the larger intensity of the band at 1643/1652 cm^{-1}, our simulated spectra are also very similar to the spectrum obtained by Jensen and Schatz[42] using a different XC functional (BP86). The main experimental RR active bands at 611, 775, 1178, 1310, 1361, 1505, and 1649 cm^{-1} are reproduced by the calculations. The main discrepancy concerns the feature/pattern around 1577 cm^{-1} as well as the relative intensities of several of the low-frequency bands. As expected from the geometrical analysis of S_1—and from the frontier orbitals dominating the excitation process—the modes presenting an enhancement in the RR spectrum mostly display motions localized on the xanthene ring as well as on the two ethylamino groups. The relative intensities of the bands in the calculated spectra show a qualitative agreement with experiment. The effect of the solvent improves the relative intensity of the bands at 1652 and 1356 cm^{-1} in ethanol, whereas it leads to an overestimation of the intensities at 1513 and 1552 cm^{-1}. On the contrary, the intensities of the bands at 614, 770, and 1180 cm^{-1} are underestimated. As a consequence, according to our calculations the discrepancies observed between the theoretical and experimental spectrum in ethanol cannot be attributed to solvation effects.

An assignment of the experimental bands is proposed in Table 3 in addition to the theoretical frequencies and the relative RR intensities calculated from eq 3. Our vibrational mode assignment is based on (i) the comparison between the modes and frequencies of Watanabe et al. (Figure 4 of ref 30) and ours, which we do not reproduce here because they are mostly identical, and (ii) the RR intensities that we calculated. Our assignment is mostly in agreement with the one proposed by Watanabe et al.[30] from comparing off-resonance, resonance, and surface-enhanced-resonance Raman scattering measurements with calculated frequencies at the B3LYP/6-311++G(d,p) level of approximation. Indeed, the experimental bands at 611, 775, 1178, 1361, 1505, and 1649 cm^{-1} are assigned to the same vibrational modes dominating the RR spectra (see Table 3).

TABLE 3: Assignment of Selected Vibrational Bands of R6G in Ethanol to One or More Vibrational Normal Modes Determined Using the B3LYP/6-311G*/IEFPCM Approach[a]

experiment	theory	
frequencies (cm^{-1})	frequencies (cm^{-1})	relative intensities
611	614[b]	0.223
775	759	0.068
	771[b]	0.189
1178	1179[b]	0.203
	1194	0.128
1310	1295	0.309
	1301	0.026
	1310[b]	0.119
1361	1354[b]	0.555
	1363	0.270
1505	1513[b]	0.725
1577	1551	0.465
	1565	0.373
	1576[b]	0.053
1649	1652[b]	1.000

[a] The relative RR intensities are calculated using the short-time approximation (eq 3). The experimental frequencies are taken from the RR scattering measurements performed in ref 30. The theoretical frequencies (cm^{-1}) have been scaled by a factor of 0.98. [b] These modes correspond to the assignment made in ref 30.

However, for the experimental bands at 775, 1178, and 1361 cm^{-1}, the calculations predict additional vibrations with non-negligible relative intensities at 759, 1194, and 1363 cm^{-1}, respectively. These modes give a noticeable contribution to the simulated RR peaks and may also be assigned to the experimental bands. Our assignment differs from the one of ref 30 for the two bands at 1310 and 1577 cm^{-1}. The band with a maximum at 1296 cm^{-1} in the simulated spectrum is obtained from the superposition of three transitions at 1295, 1301, and 1310 cm^{-1} having relative intensities of 0.309, 0.026, and 0.119, respectively. Therefore, our calculations suggest that the experimental band at 1310 cm^{-1} can mainly be assigned to the vibration at 1295 cm^{-1} with a secondary intensity arising from the vibration at 1310 cm^{-1}. Nevertheless, the discrepancy found between the maxima of the theoretical and experimental bands (14 cm^{-1}) may also suggest that the relative intensity of the modes at 1295 and 1310 cm^{-1} is inaccurately predicted by the simulation. The second difference in the assignment concerns the band at 1577 cm^{-1}, which was assigned by Watanabe et al.[30] to distortions of the phenyl ring (ω = 1576 cm^{-1}) and then later by Jensen and Schatz[42] to in-plane xanthene ring stretching and N−H bending. Our calculations rather assign this band to two modes involving motions located on the xanthene and ethylamino groups with frequencies at 1551 and 1565 cm^{-1}.

In ref 42 it has been proposed that the bands at 611 and 775 cm^{-1} may gain some intensity enhancement by a vibronic coupling mechanism. Indeed, in the experiment realized by Watanabe et al.[30] the RR spectrum has been recorded for an excitation wavelength close to the vibronic shoulder. Knowing that the relative RR intensities can be strongly affected by the position of the excitation wavelength with respect to the absorption maximum, a specific value close to the vibronic shoulder could possibly modify the intensities of the two bands at 611 and 775 cm^{-1}. In order to investigate the effect of varying the excitation wavelength, the RR spectrum of R6G in resonance with the $S_0 \rightarrow S_1$ transition was simulated for three different wavelengths corresponding to excitations in the maximum (530 nm), the vibronic shoulder (496 nm), and the post-resonance domain (457 nm), as deduced from Figure 3. These excitation wavelengths were used in the SERR spectra measured by Hildebrandt and Stockburger.[25] Figure 7 presents the calculated

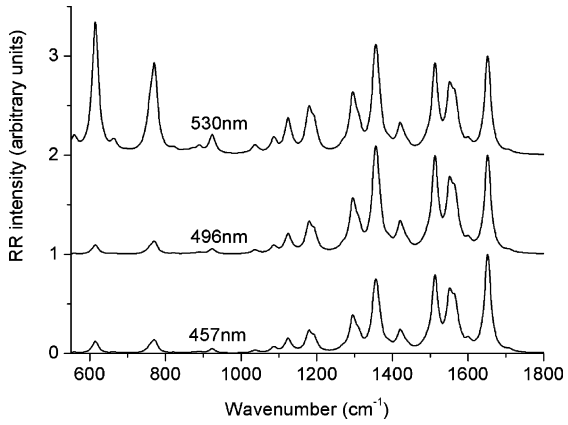

Figure 7. Simulated RR spectra of R6G in resonance with the $S_0 \rightarrow S_1$ transition in ethanol (calculated from eq 1) for three different excitation wavelengths using DFT and TDDFT methods at the B3LYP/6-311G∗ level of approximation. The RR transitions are represented by Lorentzian functions having fwhm of 20 cm^{-1} and normalized so that the intensity of the band at 1652 cm^{-1} is equal to unity. The theoretical $\omega_{e0,g0}$ origin has been shifted so that experimental and theoretical absorption maxima coincide.

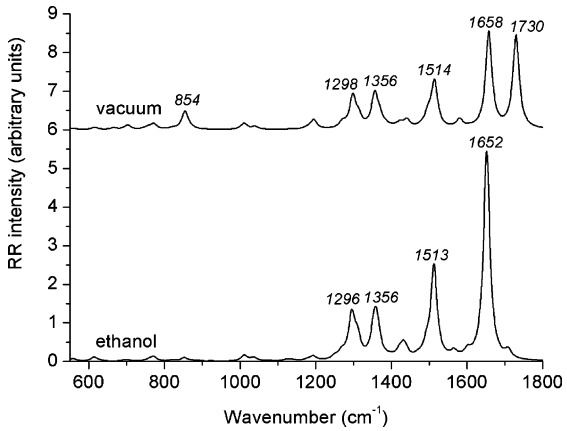

Figure 8. Simulated RR spectra of R6G in resonance with the $S_0 \rightarrow S_3$ transition in vacuum and ethanol (within the short-time approximation) using DFT and TDDFT methods at the B3LYP/6-311G∗ level of approximation. The RR transitions are represented by Lorentzian functions having fwhm of 20 cm^{-1}.

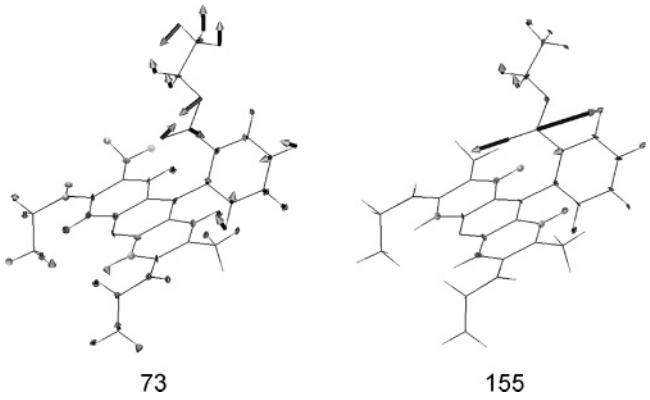

Figure 9. Pictorial representation of the normal modes 73 and 155 (B3LYP/6-311G∗).

spectra in ethanol evaluated from eq 1. The same values of $\omega_{e0,g0}$ and fwhm were used as for simulating the UV−vis absorption spectrum. Similar to Figure 6, the spectra were normalized so that the intensity of the band close to 1650 cm^{-1} is equal to unity. The spectrum obtained at 457 nm is very close to the spectrum calculated within the short-time approximation. This is due to the fact that the excitation is far from the maximum, therefore reducing the impact of the vibronic structure. For an excitation in the vibronic shoulder (496 nm), the effect of the vibronic structure remains small. The bands at 1180, 1296, and 1356 cm^{-1} gain some relative intensity, which slightly improves the agreement with the experimental spectrum reported in Figure 6. Nevertheless, the bands at 614 and 770 cm^{-1} are still found with a too weak intensity. For an excitation in the maximum of absorption (530 nm) the bands at 1180, 1296, and 1356 cm^{-1} gain some additional intensity, but the most noticeable enhancement is obtained for the bands at 614 and 770 cm^{-1}, showing the importance of vibronic coupling. If one compares our spectra with the SERR measurements given in Figure 11 of ref 25, it can be seen that the evolution of the relative intensities as a function of the wavelength is qualitatively reproduced by the calculations, though the effect of the surface is not taken into account in our simulations. Indeed, the band at 770 cm^{-1} is strongly enhanced for an excitation in the maximum, both in experiment and theory. Furthermore, inversion of the relative intensity of the bands at 1356 and 1652 cm^{-1} obtained in the simulations, when going from an excitation at 457 nm to an excitation at 530 nm, is in qualitative agreement with what is measured in the SERR of ref 25. When going from an excitation wavelength of 457 to 530 nm, the simulated relative intensities of the bands at 770 and 1356 cm^{-1} increase from 0.14 and 0.75 to 0.94 and 1.12, respectively. The simulated spectra at 457 and 530 nm are in good agreement with the SERR spectra. For an excitation in the absorption shoulder, the main disagreement concerns the band at 770 cm^{-1}, but several studies[25,26,28] have shown that the experimental SERR intensities of the bands around 611 and 775 cm^{-1} present large fluctuations, which can be explained by interactions with the surface. This is also in agreement with the SERR measurements performed at comparable excitation wavelengths.[27,29] A similar difference with experiment is noticed for the bands around 611 and 775 cm^{-1} when comparing to the RR spectrum of Watanabe et al.[30] recorded for an excitation at 488 nm. Additional simulations performed for an intermediate excitation, but not reported here, gradually recover the exaltation of the low-frequency band intensities. This demonstrates that the enhancement of these bands arises from vibronic coupling and that the approximations made in our simulation predict their appearance at larger wavelengths, i.e., at wavelengths closer to the absorption maximum.

The RR properties of the S_3 state are now considered. Similar to Figure 5, Figure 8 presents the RR spectra in vacuum and ethanol calculated from the short-time approximation expression (eq 3). Contrary to state S_1, the solvent has a large effect on the RR intensities. The intensities of the bands at 1296, 1356, 1513, and 1652 cm^{-1} significantly increase in ethanol and are in agreement with the larger ΔBL values found for this state in ethanol (Table 2). Additionally, the bands at 854 and 1730 cm^{-1} lose most of their intensities when considering ethanol as solvent. These bands correspond to the normal modes 73 and 155. As can be seen from Figure 9, they are characterized by vibrational motions localized on the ethoxy carbonyl group. Therefore, the strong sensibility of the RR intensities to the solvent can be related to the structural modifications occurring on the ethoxy carbonyl group upon excitation. From Table 2, it appears that the main differences of ΔBL values between vacuum and ethanol are obtained for the C18−C29 bond and to some extent for the C29−O30 and C29−O31 bonds. All these bonds show a decrease of their absolute ΔBL value when passing from vacuum to ethanol, which explains why modes 73 and 155 lose most of their intensities in ethanol, in agreement with the change of singly excited configuration contributions.

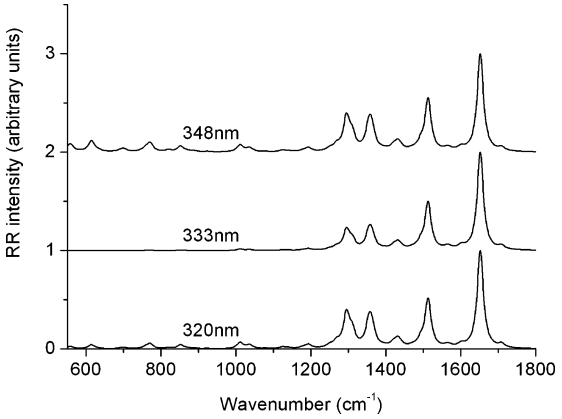

Figure 10. Simulated RR spectra of R6G in resonance with the $S_0 \rightarrow S_3$ transition in ethanol (calculated from eq 1) for three different excitation wavelengths using DFT and TDDFT methods at the B3LYP/6-311G* level of approximation. The RR transitions are represented by Lorentzian functions having fwhm of 20 cm^{-1} and normalized so that the intensity of the band at 1652 cm^{-1} is equal to unity. The theoretical $\omega_{e0,g0}$ origin has been shifted so that experimental and theoretical absorption maxima coincide.

The spectra presented for the S_3 state are clearly different than those of the S_1 state and show a strong solvent effect. Unfortunately, to our knowledge, no experimental RR measurements were performed for an excitation wavelength in resonance with this state, and therefore, no comparison to experimental results is presented.

Figure 10 presents the RR spectra of R6G in resonance with the $S_0 \rightarrow S_3$ transition in ethanol simulated for three different wavelengths corresponding to an excitation in the maximum of absorption (348 nm), the vibronic shoulder (333 nm), and the postresonant domain (320 nm). The RR spectrum of R6G in resonance with S_3 displays a weak dependence with respect to the excitation frequency. Indeed, the relative intensities of the bands at 1652 and 1513 cm^{-1} are almost not modified. The main effect is found for the bands at 1296 and 1356 cm^{-1}, which show a small reduction of their relative intensities for an excitation in the vibronic shoulder (333 nm). Moreover, the three spectra are rather similar to the one obtained within the short-time approximation (Figure 8), which confirms that the frequency dependence of the RR intensities is small for this state. The weak effect of the excitation wavelength arises from the fact that only few modes are RR active for S_3 and that they are all located in a limited frequency region (1250−1700 cm^{-1}). Therefore, they have comparable excitation profiles and their relative intensities are only slightly modified for excitations scanning the absorption spectrum.

4. Conclusions

The geometries, UV−vis absorption spectra, and RR intensities have been determined for the S_1 and S_3 excited states of R6G in vacuum and ethanol by means of DFT/TDDFT methodologies with the aim of better understanding the structures and properties of the excited states. The RR spectra have been simulated from the vibronic theory of RR scattering as well as within the short-time approximation, while the solvent effects have been modeled using the polarizable continuum model.

The S_1 and S_3 states of R6G present UV−vis absorption bands with similar vibronic structure, i.e., a shoulder at smaller wavelengths, although this shoulder is relatively more intense and more sensitive to the solvent in the case of S_3. These differences are corroborated by the larger geometry relaxations upon excitation for S_3 and the fact that the charge transfer of S_3 is reduced in ethanol. Moreover, the differences between S_1 and S_3 are magnified when considering the RR spectra. On one hand, the RR spectrum of R6G in resonance with the $S_0 \rightarrow S_1$ transition—in the 500−1800 cm^{-1} window—presents many transitions of which the relative intensities strongly vary when the excitation wavelength gets closer to the maximum of absorption. The RR spectrum of R6G in resonance with S_1 is however little influenced by the solvent. On the other hand, the RR spectrum of R6G in resonance with the $S_0 \rightarrow S_3$ transition displays only a few bands, strongly depends on the solvent, and is little affected when changing the excitation wavelength within the limits of the absorption band. As a consequence, the short-time approximation is suitable to reproduce the RR spectrum of R6G in resonance with S_3 for a broad range of excitation wavelengths, whereas the vibronic theory approach is needed for describing the RR spectrum of R6G in resonance with S_1 close to resonance.

The simulated UV−vis absorption (S_1 and S_3) and RR (S_1) spectra are globally in good agreement with experiment and substantiate the theoretical investigations by Watanabe et al.[30] and Jensen and Schatz.[42] In particular, the vibronic theory calculations confirm the assumption made in ref 42 about the vibronic coupling origin of the large intensity bands at 614 and 770 cm^{-1}. Though the surface is not modeled in our simulations, our calculations also reproduce most of the features observed in surface-enhanced measurements carried out as a function of the wavelength. Limitations of our calculations can be attributed to the quality of the XC functional, the lack of anharmonicity corrections, the approximate treatment of the solvent, and the absence of surface.

Acknowledgment. One of the authors (J.G.) thanks the Fund for Scientific Research (F.R.S.)−FNRS for his postdoctoral grant under the convention No. 2.4.509.04.F. The other author (B.C.) thanks the F.R.S.-FNRS for his research director position. The calculations have been performed on the Interuniversity Scientific Computing Facility (ISCF) installed at the Facultés Universitaires Notre-Dame de la Paix (Namur, Belgium) for which the authors gratefully acknowledge the financial support of the FNRS-FRFC and the 'Loterie Nationale' for the convention No. 2.4578.02 and of the FUNDP.

References and Notes

(1) Albrecht, A. C. *J. Chem. Phys.* **1961**, *34*, 1476.
(2) Heller, E. J.; Sundberg, R. L.; Tannor, D. *J. Phys. Chem.* **1982**, *86*, 1822.
(3) Myers, A. B. *Chem. Rev.* **1996**, *96*, 911.
(4) Kelley, A. M. *J. Phys. Chem. A* **1999**, *103*, 6891.
(5) Mennucci, B.; Cappelli, C.; Cammi, R.; Tomasi, J. *Theor. Chem. Acc.* **2007**, *117*, 1029.
(6) Jones, C. M.; Asher, S. A. *J. Chem. Phys.* **1988**, *89*, 2649.
(7) Jensen, L.; Zhao, L. L.; Autschbach, J.; Schatz, G. C. *J. Chem. Phys.* **2005**, *123*, 174110.
(8) Zhao, J.; Jensen, L.; Sung, J.; Zou, S.; Schatz, G. C.; Van Duyne, R. P. *J. Am. Chem. Soc.* **2007**, *129*, 7647.
(9) Moran, A. M.; Delbecque, C.; Kelley, A. M. *J. Phys. Chem. A* **2001**, *105*, 10208.
(10) Moran, A. M.; Bartholomew, G. P.; Bazan, G. C.; Kelley, A. M. *J. Phys. Chem. A* **2002**, *106*, 4928.
(11) Moran, A. M.; Egolf, D. S.; Blanchard-Desce, M.; Kelley, A. M. *J. Chem. Phys.* **2002**, *116*, 2542.
(12) Leng, W.; Würthner, F.; Kelley, A. M. *J. Phys. Chem. A* **2005**, *109*, 1570.
(13) Biswas, N.; Umapathy, S. *J. Chem. Phys.* **2003**, *118*, 5526.
(14) Boilet, L.; Buntinx, G.; Lapouge, C.; Lefumeux, C.; Poizat, O. *Phys. Chem. Chem. Phys.* **2003**, *5*, 834.
(15) Zeggari, S.; Lapouge, C.; Buntinx, G.; Poizat, O. *Chem. Phys.* **2005**, *313*, 113.

(16) Modeling of Vibrational Spectroscopies (Special issue) *Int. J. Quantum Chem.* **2005**, *104* (5).
(17) Quinet, O.; Champagne, B. *J. Chem. Phys.* **2002**, *117*, 2481.
(18) Botek, E.; Champagne, B. *Appl. Phys. B* **2002**, *74*, 627.
(19) Quinet, O.; Champagne, B.; Rodriguez, V. *J. Chem. Phys.* **2004**, *121*, 4705.
(20) Mani, A. A.; Schultz, Z. D.; Caudano, Y.; Champagne, B.; Humbert, C.; Dreesen, L.; Gewirth, A. A.; White, J. O.; Thiry, P. A.; Peremans, A. *J. Phys. Chem. B* **2004**, *108*, 16135.
(21) Lamparska, E.; Liégeois, V.; Quinet, O.; Champagne, B. *Chem. Phys. Chem.* **2006**, *7*, 2366.
(22) Liégeois, V.; Quinet, O.; Champagne, B.; Haesler, J.; Zuber, G.; Hug, W. *Vib. Spectrosc.* **2006**, *42*, 309.
(23) Liégeois, V.; Ruud, K.; Champagne, B. *J. Chem. Phys.* **2007**, *127*, 204105.
(24) Guthmuller, J.; Champagne, B. *J. Chem. Phys.* **2007**, *127*, 164507.
(25) Hildebrandt, P.; Stockburger, M. *J. Phys. Chem.* **1984**, *88*, 5935.
(26) Michaels, A. M.; Nirmal, M.; Brus, L. E. *J. Am. Chem. Soc.* **1999**, *121*, 9932.
(27) Li, W. H.; Li, X. Y.; Yu, N. T. *Chem. Phys. Lett.* **1999**, *312*, 28.
(28) Weiss, A.; Haran, G. *J. Phys. Chem. B* **2001**, *105*, 12348.
(29) Anger, P.; Feltz, A.; Berghaus, T.; Meixner, A. J. *J. Microsc.* **2003**, *209*, 162.
(30) Watanabe, H.; Hayazawa, N.; Inouye, Y.; Kawata, S. *J. Phys. Chem. B* **2005**, *109*, 5012.
(31) Hayazawa, N.; Inouye, Y.; Sekkat, Z.; Kawata, S. *Chem. Phys. Lett.* **2001**, *335*, 369.
(32) Hayazawa, N.; Inouye, Y.; Sekkat, Z.; Kawata, S. *J. Chem. Phys.* **2002**, *117*, 1296.
(33) Vogel, R.; Harvey, M.; Edwards, G.; Meredith, P.; Heckenberg, N.; Trau, M.; Rubinsztein-Dunlop, H. *Macromolecules* **2002**, *35*, 2063.
(34) Vogel, R.; Meredith, P.; Harvey, M. D.; Rubinsztein-Dunlop, H. *Spectrochim. Acta, Part A* **2004**, *60*, 245.
(35) Martínez Martínez, V.; López Arbeloa, F.; Bañuelos Prieto, J.; Arbeloa, López, T.; López Arbeloa, I. *J. Phys. Chem. B* **2004**, *108*, 20030.
(36) Martínez Martínez, V.; López Arbeloa, F.; Bañuelos Prieto, J.; López Arbeloa, I. *J. Phys. Chem. B* **2005**, *109*, 7443.
(37) Gavrilenko, V. I.; Noginov, M. A. *J. Chem. Phys.* **2006**, *124*, 044301.
(38) Raschke, M. B.; Hayashi, M.; Lin, S. H.; Shen, Y. R. *Chem. Phys. Lett.* **2002**, *359*, 367.
(39) Hayashi, M.; Lin, S. H.; Raschke, M. B.; Shen, Y. R. *J. Phys. Chem. A* **2002**, *106*, 2271.
(40) Heinz, T. F.; Chen, C. K.; Ricard, D.; Shen, Y. R. *Phys. Rev. Lett.* **1982**, *48*, 478.
(41) Lin, S. H.; Alden, R. G.; Villaeys, A. A.; Pflumio, V. *Phys. Rev. A* **1993**, *48*, 3137.
(42) Jensen, L.; Schatz, G. C. *J. Phys. Chem. A* **2006**, *110*, 5973.
(43) Peticolas, W. L.; Rush, T., III. *J. Comput. Chem.* **1995**, *16*, 1261.
(44) Duschinsky, F. *Acta Physicochim. URSS* **1937**, *7*, 551.
(45) Rush, T., III; Kumble, R.; Mukherjee, A.; Blackwood, M. E., Jr.; Spiro, T. G. *J. Phys. Chem.* **1996**, *100*, 12076.
(46) Lee, S. Y.; Heller, E. J. *J. Chem. Phys.* **1979**, *71*, 4777.
(47) Heller, E. J. *Acc. Chem. Res.* **1981**, *14*, 368.
(48) Hassing, S.; Mortensen, O. S. *J. Chem. Phys.* **1980**, *73*, 1078.
(49) Neugebauer, J.; Hess, B. A. *J. Chem. Phys.* **2004**, *120*, 11564.
(50) Frisch, M. J.; Trucks, G. W.; Schlegel, H. B.; Scuseria, G. E.; Robb, M. A.; Cheeseman, J. R.; Montgomery, J. A., Jr.; Vreven, T.; Kudin, K. N.; Burant, J. C.; Millam, J. M.; Iyengar, S. S.; Tomasi, J.; Barone, V.; Mennucci, B.; Cossi, M.; Scalmani, G.; Rega, N.; Petersson, G. A.; Nakatsuji, H.; Hada, M.; Ehara, M.; Toyota, K.; Fukuda, R.; Hasegawa, J.; Ishida, M.; Nakajima, T.; Honda, Y.; Kitao, O.; Nakai, H.; Klene, M.; Li, X.; Knox, J. E.; Hratchian, H. P.; Cross, J. B.; Bakken, V.; Adamo, C.; Jaramillo, J.; Gomperts, R.; Stratmann, R. E.; Yazyev, O.; Austin, A. J.; Cammi, R.; Pomelli, C.; Ochterski, J. W.; Ayala, P. Y.; Morokuma, K.; Voth, G. A.; Salvador, P.; Dannenberg, J. J.; Zakrzewski, V. G.; Dapprich, S.; Daniels, A. D.; Strain, M. C.; Farkas, O.; Malick, D. K.; Rabuck, A. D.; Raghavachari, K.; Foresman, J. B.; Ortiz, J. V.; Cui, Q.; Baboul, A. G.; Clifford, S.; Cioslowski, J.; Stefanov, B. B.; Liu, G.; Liashenko, A.; Piskorz, P.; Komaromi, I.; Martin, R. L.; Fox, D. J.; Keith, T.; Al-Laham, M. A.; Peng, C. Y.; Nanayakkara, A.; Challacombe, M.; Gill, P. M. W.; Johnson, B.; Chen, W.; Wong, M. W.; Gonzalez, C.; Pople, J. A. *Gaussian 03*, Revision C.02; Gaussian, Inc.: Wallingford, CT, 2004.
(51) Becke, A. D. *J. Chem. Phys.* **1993**, *98*, 5648.
(52) Lee, C.; Yang, W.; Parr, R. G. *Phys. Rev. B* **1988**, *37*, 785.
(53) Tomasi, J.; Mennucci, B.; Cammi. R. *Chem. Rev.* **2005**, *105*, 2999.
(54) Cammi, R.; Mennucci. B. *J. Chem. Phys.* **1999**, *110*, 9877.
(55) Cossi, M.; Barone, V. *J. Chem. Phys.* **2001**, *115*, 4708.
(56) Du, H.; Fuh, R. A.; Li, J.; Corkan, A.; Lindsey, J. S. *Photochem. Photobiol.* **1998**, *68*, 141.
(57) Guillaume, M.; Champagne, B.; Zutterman, F. *J. Phys. Chem. A* **2006**, *110*, 13007.